# 4.05 kW monolithic fiber laser oscillator based on home-made large mode area fiber Bragg gratings

**Baolai Yang (杨保来)[1], Hanwei Zhang (张汉伟)[1,2,3], Qing Ye (叶青)[4],**
**Haoyang Pi (皮浩洋)[4], Chen Shi (史尘)[1,2,3], Rumao Tao (陶汝茂)[1,2,3],**
**Xiaolin Wang (王小林)[1,2,3], and Xiaojun Xu (许晓军)[1,2,3,\*]**

[1]*College of Advanced Interdisciplinary Studies, National University of Defense Technology, Changsha 410073, China*
[2]*Hunan Provincial Key Laboratory of High Energy Laser Technology, Changsha 410073, China*
[3]*Hunan Provincial Collaborative Innovation Center of High Power Fiber Laser, Changsha 410073, China*
[4]*Shanghai Institute of Optics and Fine Mechanics, Chinese Academy of Sciences, Shanghai 201800, China*
*\*Corresponding author: xu_xiaojun@126.com*

With the increasing output power of the monolithic fiber laser oscillators, the stimulated Raman scattering (SRS) effect becomes one of the main limitations of power scaling. Employing fiber with a larger mode area is an effective technique to mitigate the SRS, but, for the monolithic fiber laser oscillators, the difficulty of the inscription of the high-reflection fiber Bragg gratings (FBGs) increases with the fiber mode area. In this work, we demonstrated a high-power monolithic fiber laser oscillator based on the home-made large mode area FBGs and ytterbium-doped fiber (YDF) with 25 μm core diameters. A maximum output power of 4.05 kW is achieved at the central wavelength of ∼1080 nm with a total 915 nm pump power of ∼6.7 kW. At the operation of 4.05 kW, the intensity of the Raman Stokes light is ∼25 dB below the signal laser, and the beam quality ($M^2$-factor) is ∼2.2. To the best of our knowledge, this is the first detailed report of the monolithic fiber laser oscillator with an output power beyond 4 kW.

*OCIS Codes: 140.3510, 140.3615, 060.3735.*
*doi: 10.3788/COL201816.031407.*

High-power fiber lasers have been widely adopted in industrial applications for the advantages of high conversion efficiency, good beam quality, easy heat management, stability, and robustness[1,2]. Generally, a high-power fiber laser can be achieved based on two structures, which are the master oscillator power amplification (MOPA) and the single-cavity fiber laser oscillator. Although there have been tremendous demonstrations on high-power fiber MOPA[3–9], the high-power fiber laser oscillators enjoy the advantages of simpler structure and fewer components when compared with the MOPA structure. However, more rigorous power handling ability and spectral bandwidth of the fiber Bragg gratings (FBGs) are required for the direct high-power operation. Benefiting from the matured large mode area (LMA) FBG inscription techniques[10–12], the output powers of the monolithic fiber laser oscillator have increased remarkably during the last years. In 2012, a monolithic fiber laser oscillator with output power of ∼1 kW was reported based on ytterbium-doped fiber (YDF) with a core/inner-cladding diameter of 20/400 μm and 915 nm laser diodes (LDs)[13]. Later in 2014, Yu *et al.* of our group reported a 1.5 kW monolithic fiber laser oscillator in a similar scheme[14]. The stimulated Raman scattering (SRS) effect was obviously observed at the operation of 1.5 kW, and further power scaling was limited. In 2016, our group effectively mitigated the SRS by employing a short gain fiber as well as the bidirectional 976 nm pump scheme[15]. A maximum output power of 2.5 kW was achieved in the monolithic fiber laser oscillator

with a Raman Stokes intensity of ∼20 dB below the signal. For further power scaling of the fiber laser oscillator, other mitigation techniques of SRS are required.

Theoretically, it is a most effective technique to mitigate the SRS by increasing the mode area of the high-power fiber lasers[16,17]. In consideration of the LMA FBG manufacture techniques, most reported high-power monolithic fiber laser oscillators employed gain fiber with a core/inner-cladding diameter of 20/400 μm and corresponding FBGs, which are commercially available and ensure a near-diffraction-limited beam quality[13–15,18,19]. However, as the output power gradually increases, the fiber laser oscillators based on gain fiber with core diameter of ∼20 μm face severe limitation of SRS in the power scaling[14,15]. In 2017, the researchers in Fujikura Inc. reported a 3 kW monolithic fiber laser oscillator based on their specially designed YDF with a mode area of ∼400 μm$^2$ and corresponding FBGs[20]. Remarkable SRS suppression was achieved with such an LMA fiber. For further power scaling, it is promising to mitigate the SRS by further increasing the fiber mode area, as long as the LMA FBGs are available.

In this letter, we report a monolithic fiber laser oscillator with a maximum output power of ∼4.05 kW, which is realized based on home-made LMA FBGs and YDF with a core/inner-cladding diameter of 25/400 μm. The LMA FBGs are manufactured with the phase mask method and operate at the central wavelength of ∼1080 nm. By employing high-power 915 nm LDs and a bidirectional-pump

scheme, the output power of the monolithic fiber laser oscillator was scaled to 4.05 kW with the intensity of Raman Stokes light ~25 dB below the signal laser.

High-power LMA FBGs are key components of the monolithic fiber laser oscillators, and their inscription is crucial to the high-power handling ability. By utilizing the phase mask technique with a KrF excimer laser as a UV light source[12,21], we inscribed a pair of FBGs on the double cladding fiber with a core/inner-cladding diameter of 25/400 μm at the Shanghai Institute of Optics and Fine Mechanics, Chinese Academy of Sciences. The high-reflectivity (HR) FBG provides a reflectivity of ~99% at the central wavelength of ~1080 nm with a 3 dB bandwidth of ~2 nm. The output coupler (OC) FBG provides a reflectivity of ~10% at the central wavelength of ~1080 nm with a 3 dB bandwidth of ~1 nm. Based on the home-made FBGs, a bidirectional-pumped monolithic fiber laser oscillator was constructed to test the performance in high-power operation. The experimental setup of the monolithic fiber laser oscillator is depicted in Fig. 1.

The pump source is high-power 915 nm LDs, which have pigtailed fiber with a core/cladding diameter of 220/240 μm. Each LD module provides a maximum pump power of ~750 W. The co-pumping LDs are combined by a 7 × 1 tapered fused bundle (TFB) combiner with seven identical pump ports. The counter-pumping LDs are combined by a (6 + 1) × 1 pump/signal combiner, which consists of six pump ports and one signal port with a core diameter of 25 μm and a numerical aperture (NA) of 0.065. In our previous work on the 976-nm-pumped high-power monolithic fiber laser oscillators[15,18], the occurrence of the transverse mode instability (TMI) usually leads to a roll-over output power and limits further power scaling. The 915 nm pumping has a moderate absorption in the YDF compared with the 976 nm pumping we employed in some previous work with observation of the TMI[18,22,23]. The bidirectional-pump configuration also distributes the heat load more evenly than the single-end-pump configurations, and thus further enhances the TMI threshold[15,24]. Besides, according to previous studies[25], the bidirectional-pump configuration enjoys the advantage of suppressing the SRS. Both of the TFB combiners couple the pump light into the inner cladding of the double cladding output fiber with a diameter of 400 μm and an NA of
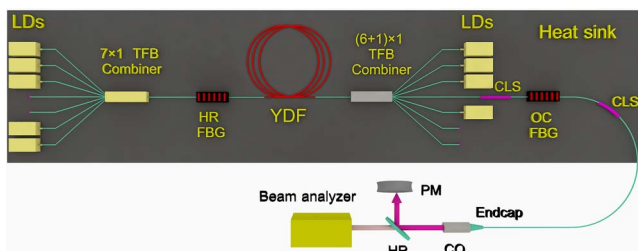
0.46. The unoccupied pump ports of the TFB combiners are angle cleaved to avoid facet reflection. The gain fiber is a commercial double-cladding YDF with a 25 μm/0.065 NA core and a 400 μm/0.46 NA inner cladding. The absorption coefficient of the YDF at 915 nm is ~0.65 dB/m, and the length of the YDF is adopted as ~33 m to absorb the most pump power. The gain fiber is coiled in circles and placed on the heat sink. The inner circles have a minimum diameter of ~12 cm, and the outer circles have a maximum diameter of ~16 cm, which could also help increase the threshold of TMI[26,27]. Two cladding light strippers (CLSs) are utilized on the both sides of the OC FBG in the fiber laser oscillator to fully dump the cladding light. After the OC FBG, an ~7 m delivery fiber with a core/inner-cladding diameter of 25/400 μm is utilized, and an endcap is employed to eliminate facet reflection. All of the components including YDF, LDs, TFB combiners, FBGs, and CLSs are placed on a water-cooled heat sink to carry away the heat accumulation. In the experiment, the output powers, optical spectra, temporal characteristics, and beam quality of the monolithic fiber laser oscillator are recorded. The temporal characteristic of the output laser is measured by utilizing a photodetector with a bandwidth of 150 MHz, and the beam quality of the output laser is measured with a beam propagation analyzer ($M^2$-200).

In the experiment, the dependence of the output power on the pump power is first measured, which is shown in Fig. 2(a). The output power of the fiber laser oscillator increases almost linearly along with the pump power.
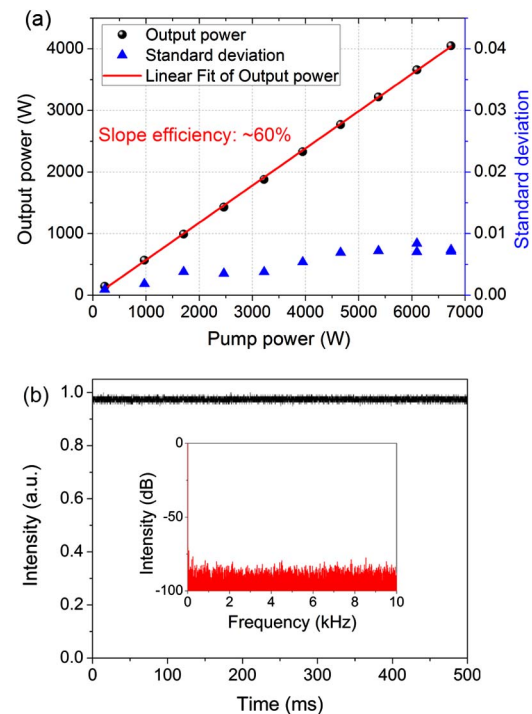


Fig. 2. (a) Output power and standard deviation of the temporal signals at different pump powers, (b) the temporal signal of the output laser and its Fourier spectrum at the operation of 4.05 kW.



Fig. 1. Experimental setup (LDs, laser diodes; YDF, ytterbium-doped fiber; CLS, cladding light stripper; CO, collimator; PM, power meter; HR, high reflector).

A maximum output power of 4.05 kW is achieved at the pump power of ~6.7 kW. The linearly fitted slope efficiency of the fiber laser oscillator is ~60%. No obvious evidence of roll-over output power or laser efficiency is observed in the power scaling process. The maximum output power is limited by the available pump power. During the power scaling process, the temporal signals of the output laser are recorded with a photodetector at different power levels. The standard deviations of the temporal signals are also shown in Fig. 2(a). In this work, despite a higher output power of 4 kW being achieved, no evidence of occurrence of the TMI is observed. We believe this is mainly attributed to employing the bidirectional 915 nm pumping scheme. The standard deviation of the temporal signals can be employed to quantify the temporal stability of the output laser and verify the occurrence of TMI in the power scaling[28–30]. During the power scaling process, all of the standard deviations of the temporal signals are below 0.01, and no remarkable increase of the standard deviations is observed. Figure 2(b) shows the temporal signal at the operation of 4.05 kW and its Fourier spectrum (the inset). The temporal signal is quite stable, and there is no typical modulation frequency of TMI observed in the Fourier spectrum[15,18,28]. From the evidence of temporal characteristics of the output laser, the absence of TMI can be confirmed in the monolithic fiber laser oscillator. Since there is unoccupied pump ports in the TFB combiners, further power scaling can be achieved if more pump power is available.

The optical spectra of the output laser at different power levels are depicted in Fig. 3. Since two CLSs are utilized, the residual pump light is stripped, and no pump light is observed in the optical spectra. The optical spectra of the signal laser broaden remarkably with the power scaling. At the operation of 140 W, the full width at half-maximum (FWHM) bandwidth of the signal laser is ~0.5 nm. When the monolithic fiber laser oscillator operates at ~4.05 kW, the FWHM bandwidth of the signal laser broadens to ~3.4 nm. The laser spectral broadening is mainly due to the fiber nonlinear effects, such as self-phase modulation (SPM)[31,32]. As we can see in Fig 3, Raman–Stokes light is observed at the operation of
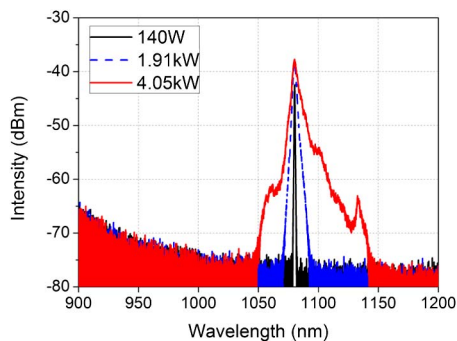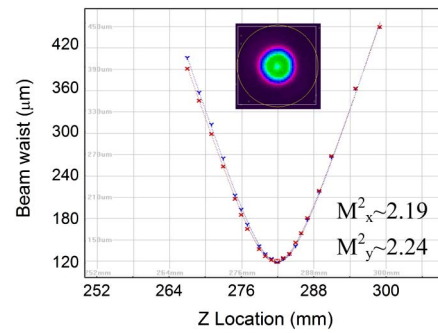


Fig. 4. Beam quality of the output laser.

~4.05 kW, and the intensity is around 25 dB below the signal laser. Compared with the reported optical spectra of the fiber laser oscillator employing gain fiber with an ~20 μm core diameter[14,15,18], the SRS is remarkably mitigated by employing the LMA fiber with a 25 μm core diameter.

The beam quality of the output laser is also measured with a beam quality analyzer ($M^2$-200). The measured $M^2$-factors and beam profile at the beam waist are shown in Fig. 4. At the operation of ~4 kW, the $M^2$-factors are ~2.2 on both axes. In this study, the adopted LMA fiber has a core diameter of 25 μm and an NA of 0.065, which correspond to a $V$ parameter of ~4.7 at the operation of ~1080 nm. Since several high-order modes are supported in the LMA fiber, it is common that the output laser contains some high-order mode content. Due to the lack of mode discrimination techniques that can be incorporated in the fiber laser oscillator, the beam quality of the output laser can be acceptable. Despite the high-order modal content causing the deterioration of the beam quality of the output laser, the existence of the high-order modes helps to mitigate the SRS, owing to the relatively larger mode area of the high-order modes than the fundamental mode.

In summary, we have demonstrated a monolithic fiber laser oscillator with a maximum output power of 4.05 kW based on an LMA YDF with a core/inner-cladding diameter of 25/400 μm and corresponding home-made LMA FBGs. The LMA FBGs were inscribed by the phase mask method and operated at ~1080 nm. High-power 915 nm LDs were employed as the pump source and distributed in a bidirectional-pump configuration. The output power of the monolithic fiber laser oscillator was scaled to 4.05 kW with a slope efficiency of ~60% without any evidence of TMI. At the operation of 4.05 kW, the FWHM spectral bandwidth of the signal laser was ~3.4 nm, and the intensity of the Raman–Stokes light was ~25 dB below the signal laser. To the best of our knowledge, this is the first detailed report of the monolithic fiber laser oscillator with output power beyond 4 kW.



Fig. 3. Optical spectra of the output laser at different power levels.

## References

1. C. Jauregui, J. Limpert, and A. Tünnermann, Nat. Photon. **7**, 861 (2013).
2. M. N. Zervas and C. A. Codemard, IEEE J. Sel. Top. Quantum Electron. **20**, 219 (2014).
3. E. Stiles, in *Proceedings of the 5th International Workshop on Fiber Lasers* (2009).
4. J. Liu, K. Liu, F. Tan, and P. Wang, IEEE J. Sel. Top. Quantum Electron. **20**, 278 (2014).
5. H. Xiao, J. Leng, H. Zhang, L. Huang, J. Xu, and P. Zhou, Appl. Opt. **54**, 8166 (2015).
6. Q. Xiao, P. Yan, D. Li, J. Sun, X. Wang, Y. Huang, and M. Gong, Opt. Express **24**, 6758 (2016).
7. C. Shi, X. Wang, P. Zhou, and X. Xu, Chin. Opt. Lett. **15**, 110605 (2017).
8. M. Jiang, P. Ma, L. Huang, J. Xu, P. Zhou, and X. Gu, High Power Laser Sci. Eng. **5**, e30 (2017).
9. C. Yang, Y. Ju, B. Yao, Z. Zhang, T. Dai, and X. Duan, Chin. Opt. Lett. **14**, 061403 (2016).
10. K. O. Hill and G. Meltz, J. Lightwave Technol. **15**, 1263 (1997).
11. S. J. Mihailov, D. Grobnic, C. W. Smelser, P. Lu, R. B. Walker, and H. Ding, Opt. Mater. Express **1**, 754 (2011).
12. W. Mohammed and X. Gu, Appl. Opt. **49**, 5297 (2010).
13. Y. Xiao, F. Brunet, M. Kanskar, M. Faucher, A. Wetter, and N. Holehouse, Opt. Express **20**, 3296 (2012).
14. H. Yu, X. Wang, R. Tao, P. Zhou, and J. Chen, Appl. Opt. **53**, 8055 (2014).
15. B. Yang, H. Zhang, C. Shi, X. Wang, P. Zhou, X. Xu, J. Chen, Z. Liu, and Q. Lu, Opt. Express **24**, 27828 (2016).
16. C. Jauregui, J. Limpert, and A. Tünnermann, Proc. SPIE **7914**, 791408 (2011).
17. J. W. Dawson, M. J. Messerly, R. J. Beach, M. Y. Shverdin, E. A. Stappaerts, A. K. Sridharan, P. H. Pax, J. E. Heebner, C. W. Siders, and C. P. J. Barty, Opt. Express **16**, 13240 (2008).
18. B. Yang, H. Zhang, X. Wang, R. Su, R. Tao, P. Zhou, X. Xu, and Q. Lu, J. Opt. **18**, 105803 (2016).
19. H. Yu, D. A. V. Kliner, K. Liao, J. Segall, M. H. Muendel, J. J. Morehead, J. Shen, M. Kutsuris, J. Luu, J. Franke, K. Nguyen, D. Woods, F. Vance, D. L. Vecht, D. Meng, R. Duesterberg, L. Xu, J. Skidmore, M. Peters, N. Guerin, J. Guo, J. Cheng, J. Du, B. Johnson, D. Yin, A. Hsieh, P. Cheng, A. Demir, J. Cai, R. Gurram, K. Lee, R. Raju, D. Zou, R. Srinivasan, M. Saini, L. Zavala, V. Rossin, E. P. Zucker, H. Ishiguro, and H. Sako, Proc. SPIE **8237**, 82370G (2012).
20. S. Ikoma, H. K. Nguyen, M. Kashiwagi, K. Uchiyama, K. Shima, and D. Tanaka, Proc. SPIE **10083**, 100830Y (2017).
21. Q. Lou, in *International Photonics and Opto Electronics Meetings* (2014), paper JF1A.2.
22. R. Tao, P. Ma, X. Wang, P. Zhou, and Z. Liu, J. Opt. **17**, 45504 (2015).
23. A. V. Smith and J. J. Smith, Opt. Express **21**, 15168 (2013).
24. R. Tao, P. Ma, X. Wang, and P. Zhou, Laser Phys. Lett. **14**, 25002 (2017).
25. P. Yan, Y. Huang, J. Sun, D. Li, X. Wang, and Q. Xiao, Laser Phys. Lett. **14**, 80001 (2017).
26. P. Ma, R. Tao, R. Su, X. Wang, P. Zhou, and Z. Liu, Opt. Express **24**, 4187 (2016).
27. R. Tao, R. Su, P. Ma, X. Wang, and P. Zhou, Laser Phys. Lett. **14**, 25101 (2017).
28. H. Otto, F. Stutzki, F. Jansen, T. Eidam, C. Jauregui, J. Limpert, and A. Tünnermann, Opt. Express **20**, 15710 (2012).
29. F. Beier, C. Hupel, J. Nold, S. Kuhn, S. Hein, J. Ihring, B. Sattler, N. Haarlammert, T. Schreiber, R. Eberhardt, and A. Tünnermann, Opt. Express **24**, 6011 (2016).
30. F. Beier, M. Plötner, B. Sattler, F. Stutzki, T. Walbaum, A. Liem, N. Haarlammert, T. Schreiber, R. Eberhardt, and A. Tünnermann, Opt. Lett. **42**, 4311 (2017).
31. S. I. Kablukov, E. A. Zlobina, E. V. Podivilov, and S. A. Babin, Opt. Lett. **37**, 2508 (2012).
32. W. Liu, P. Ma, H. Lv, J. Xu, P. Zhou, and Z. Jiang, Opt. Express **24**, 26715 (2016).